DOI: 10.26599/FSHW.2026.9251117

Contents lists available at SciOpen

Food Science and Human Wellness

journal homepage: https://www.sciopen.com/journal/2097-0765

China Food Publishing Co.

Pectin molecular weight as a key determinant for designing functional yogurt textures: toward personalized nutrition

Zhipeng Su[a,c,d], Zixuan Li[a,c,d], Lingtao Kang[a,c,d], Weiqing Zhang[a,c,d], Yifei Zhao[a,c,d], Xia Chang[c,d], Yujiao Qian[a,c,d], Fan Huang[c,d], Xiaopeng Li[c,d], Hong-Hui Wang[b,*], Gaoyang Li[a,c,d,*]

[a] *Longping Agricultural College, Hunan University, Changsha 410125, China.*

[b] *College of Biology, Hunan University, Changsha 410082, China*

[c] *Hunan Institute of Agricultural Product Processing and Quality Safety, DongTing Laboratory, Hunan Academy of Agricultural Sciences, Changsha 410125, China.*

[d] *Hunan Key Lab of Fruits & Vegetables Storage, Processing, Quality and Safety, Hunan Institute of Agricultural Product Processing and Quality Safety, Changsha 410125, China.*

ABSTRACT: The texture of soft materials, such as yogurt, emerges from the complex interplay of their constituent molecules. While polysaccharides are widely used to modulate texture, achieving predictable outcomes is hindered by their structural heterogeneity. Here, we demonstrate that pectin molecular weight (Mw) acts as a master regulator for designing customizable yogurt textures through precise control of casein network assembly. By fractionating lemon pectin into discrete MW fractions, we achieved distinct viscoelastic landscapes in yogurt systems: intermediate Mw (20.01 kDa) induced weak, flowable gels by disrupting optimal pectin-protein interactions (electrostatic and hydrophobic interactions), whereas high and lower Mw (40.09 and 7.77 kDa) reinforced the network through enhanced protein-protein binding (disulfide bonding). This reveals a non-monotonic (U-shaped) dependence of gel strength on pectin chain length. Our findings provide a mechanistic framework for Mw-directed texture engineering, offering practical guidelines for developing texture-tunable foods tailored for vulnerable populations, such as the elderly and individuals with dysphagia. This work thereby advances the intersection of food science and human wellness.

Keywords: Yogurt texture customization, pectin–protein interactions, stability enhancement, functional foods, and dysphagia nutrition.

1. Introduction

Yogurt is a highly nutritious dairy product widely consumed worldwide, valued for its health benefits including probiotic delivery and improved nutrient bioavailability [1,2]. Nevertheless, the yogurt industry faces dual challenges: internally, technological limitations such as syneresis (whey separation) during fermentation and storage compromise product stability and consistency [3,4]; externally, evolving consumer preferences demand diverse textural experiences beyond conventional set-type and stirred-type yogurts, including products tailored for specific dietary needs like dysphagia or healthy aging [5]. Enhancing yogurt

***Corresponding author**
lgy7102@163.com (G. Y. Li);
wanghonghui@hnu.edu.cn (H. H. Wang)

Received 10 November 2025
Received in revised from 16 December 2025
Accepted 19 March 2026

stability is therefore crucial for sustainable industry development and for meeting broad consumer health expectations [6]. Therefore, developing a versatile strategy to precisely tailor yogurt texture is essential to address both technical stability and personalized consumer requirements. The fundamental mechanism underlying instability involves casein aggregation and rearrangement, which drive serum expulsion from the gel network [7,8]. Current research shows that various additives can improve stability through casein interactions: Ca^{2+} reinforces gel structure via electrostatic screening and calcium bridging [9,10]; whey protein and gelatin stabilize the matrix through disulfide bonds and hydrogen bonding [11,12]; while chitosan and soy protein fibrils enhance stability via electrostatic interactions [13]. Although these additives effectively promote gelation and mitigate stability concerns, achieving targeted texture diversity while upholding consumer-friendly formulations and health-oriented formulations remains a significant challenge to satisfy increasingly heterogeneous market and wellness demands.

Compared to salts and proteins which can induce texture hardening and allergenic responses, polysaccharides represent more consumer-friendly modifiers [14,15]. Among them, pectin, with its inherent attributes as a natural, soluble dietary fiber, demonstrates unique advantages in developing yogurt with enhanced stability, reduced caloric content, and improved nutritional value, aligning more closely with modern health-conscious dietary preferences [16,17]. However, the application of pectin is constrained by its significant structural heterogeneity, which includes variations in backbone configuration (primarily HG, RG-I, and RG-II) [18] and degree of esterification (high-methoxyl >50% vs. low-methoxyl <50%) [19]. These structural divergences lead to unpredictable textural outcomes: for instance, RG-I and low-ester pectin can form stable gels via interactions with casein, whereas high-ester pectin often results in liquid yogurt [4,20]. Despite the profound impact of these structural features, their inherent complexity often leads to convoluted structure-function relationships, making it difficult to use them as simple engineering handles. Consequently, the precise engineering of gel macroscopic properties by tuning a single molecular parameter remains a critical challenge for achieving precision nutrition and personalized diets [21–23]. Within this context, the role of MW, a more readily tunable parameter, has been largely overlooked. However, we propose that Mw could serve as a singular governing parameter for texture design, offering higher predictability than complex chemical substitutions. Previous studies hint at its potential; for example, ultrasonically modulating the molecular weight of chitosan enables texture customization of yogurt for 3D printing applications [24]. Similarly, the MW of pectin directly governs its viscosity and gelling properties [25–27].

This study establishes MW as a primary determinant for customizing yogurt texture, thereby introducing a novel paradigm for developing functional foods tailored to specific health needs. We challenge the prevailing complexity in pectin structure-function relationships by hypothesizing that Mw serves as a more robust predictor of texture modality than fine structural parameters like degree of esterification, enabling the construction of a texture design framework aligned with precision nutrition. Our work seeks to isolate and highlight the dominant effect of Mw by minimizing the covariation of other structural parameters, thereby establishing a principal control parameter for personalized yogurt texture customization (**Scheme 1**).

Critically, our investigation uncovers a non-monotonic, U-shaped relationship between pectin Mw and key yogurt texture parameters, where both high and low Mw fractions promote firm gel formation through distinct mechanisms, while an intermediate Mw results in a notably weaker, more fluid structure. By systematically fractionating lemon pectin (LP20-LP80), we not only evaluated its macro-properties but also mechanistically decoded their differential regulatory effects on yogurt quality. This establishes a clear logical progression from molecular fractionation to mechanistic understanding and final functional application, especially those meeting rheological criteria for dysphagia diets, suggest potential for developing personalized dairy products for vulnerable populations, though clinical and sensory validation remains necessary.

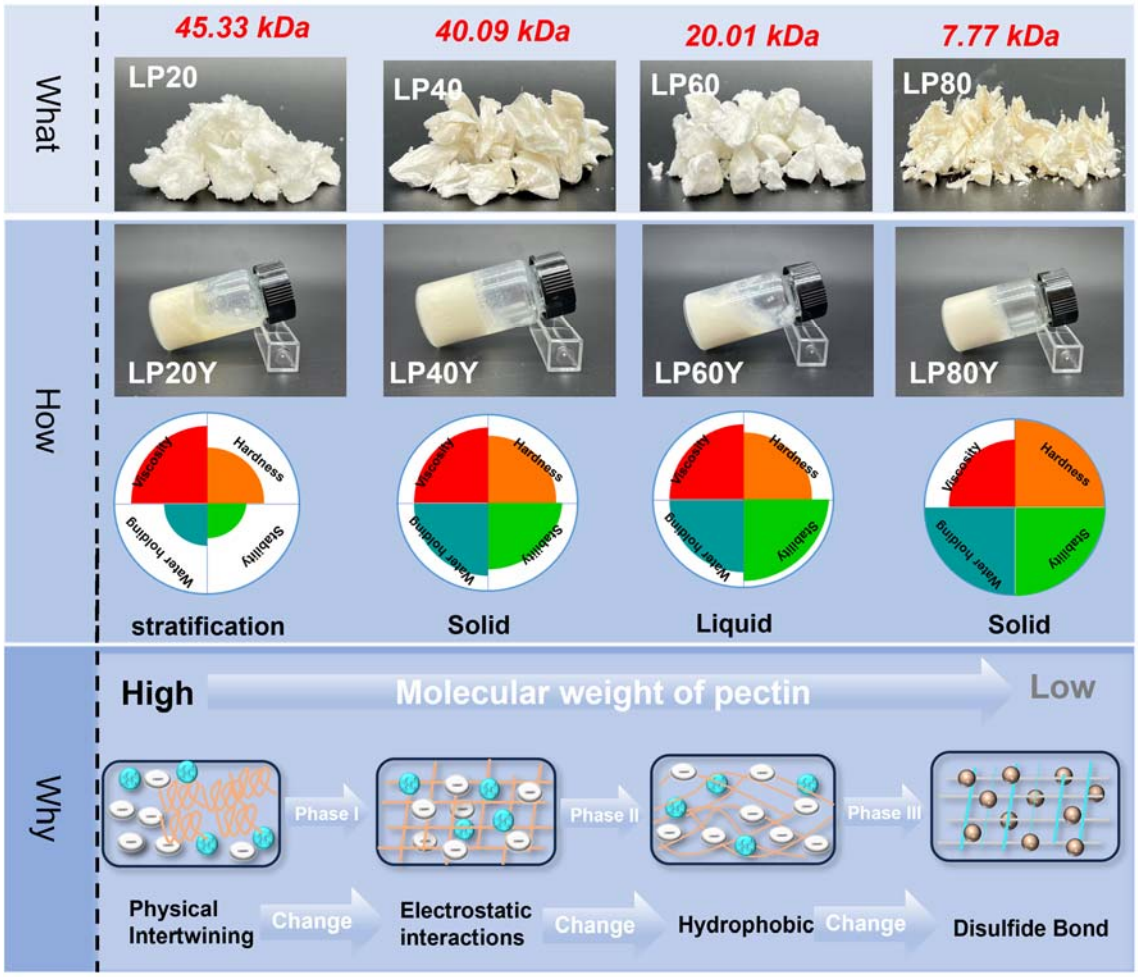

Scheme 1. Conceptual framework for MW-based texture customization in yogurt. Lemon pectin (LP) was fractionated by ethanol precipitation (yielding LP20, LP40, LP60, LP80). Yogurt fortified with these fractions is termed LPY, with corresponding labels (e.g., LPY20).

2. Materials and methods

2.1 Materials

Lemon (Citrus Eureka) fruits were sourced from supermarkets in Hunan, China. The peels were extracted, dehydrated, and processed to a 60-mesh consistency. The peel powder was then macerated in a 95% ethanol solution at a 1:20 (w/v) ratio for 12 h, repeated thrice. The insoluble residues were subsequently air-dried at 50 °C for 24 h. All reagents were of analytical grade and used as received. All aqueous solutions

were prepared using ultrapure water (organic-free, 18.2 MΩ cm resistance) from a Milli-Q system (Millipore, Billerica, USA).

2.2 Yield and purity of LP fractions

The protein content of the four fractions was assessed by coomassie brilliant blue staining (with bovine serum albumin as a reference)[28]. The uronic acid content was determined using the carbazole-sulfuric method with glucuronic acid as a standard (530 nm) [29]. The total sugar of samples was measured by phenol-sulfuric acid (with Glucose as a standard)[30]. Moreover, the total polyphenol of samples was assessed by Folin-Ciocalteu (with Gallic acid as a standard)[31]. The UV–vis spectrum was measured on a UV–visible spectrophotometer (UV2600, Shimadzu, Kyoto, Japan). The yields of four LP fractions were calculated according to Eq.

Yield% = m1/m × 100%

where m was the dry weight of LP before separation (g) and m1 was the dry weight of the individual LP fractions (g).

2.3 Preparation of pectin by gradient ethanol precipitation

The crude pectin was first extracted from dried lemon peel with acidified water (pH adjusted to 3.0 using citric acid) at 85 °C for 2 h, followed by filtration, alcohol precipitation, and drying. The LP fractions were isolated using an established ethanol fractionation method [32]. Briefly, 500 mL of LP solution (10 mg/mL) was placed in a constant-temperature magnetic stirring bath. Anhydrous ethanol was added dropwise (approximately 2 mL/min) under constant stirring until a final concentration of 20% (v/v) was reached. The mixture was allowed to equilibrate at 4 °C for 24 h to ensure complete precipitation of the first fraction. The precipitate was collected by centrifugation at 4 °C (6,000 ×g, 30 min) and labeled as LP20. Subsequently, the resulting supernatant was further adjusted to 40% (v/v) ethanol concentration following the same procedure to yield LP40. This sequential process was repeated to achieve final concentrations of 60% and 80% (v/v), yielding LP60 and LP80, respectively [33] (**Figure S1**). All collected precipitates were redissolved in ultrapure water, dialyzed (MWCO: 3,500 Da) against distilled water for 48 h to remove residual ethanol and salts, and finally lyophilized to yield four distinct pectin fractions.

2.4 Molecular weight analysis

The molecular weights of the LP fractions were precisely determined using gel permeation chromatography (GPC), integrated into a high-performance liquid chromatography (HPLC) system (Shimadzu, Kyoto, Japan). The analytical setup was equipped with a differential refractive index detector (RI-10A, RefractoMax520, Thermo Fisher, MA, USA) and utilized an Ultrahydrogel linear column (7.8 mm × 300 mm) in conjunction with an Ultrahydrogel Guard Column (6 mm × 40 mm). The elution was facilitated by a 0.1 mmol/L NaCl solution, which was delivered at a flow rate of 0.6 mL/min, with the system temperature consistently maintained at 35 °C. The aliquot volume for sample injections was standardized to 10 μL at a concentration of 2 mg/mL. For the construction of the calibration curve, a series of dextran standards with

molecular weights ranging from 5, 15, 270, 410, 670 kDa was employed. The reported molecular weights are relative values based on dextran calibration and are used for comparative analysis within this study. A linear regression equation, Log MW = -1.773 × X + 23.300, was formulated for the estimation of molecular weights, where X denotes the peak elution time, achieving a coefficient of determination (R^2) of 0.9943 (**Figure S2**). The polydispersity index, which is the ratio of the weight-average molecular weight (Mw) to the number-average molecular weight (Mn), was calculated to provide insights into the molecular weight distribution of the pectin samples (Mw/Mn).

2.5 Determination of esterification degree

As previously reported, the degree of esterification of LP can be preliminarily estimated using FT-IR spectroscopy, which is the ratio of the peak area at 1740 cm^{-1} (A_{1740}) to the sum of the peak areas at 1740 cm^{-1} and 1610 cm^{-1} (A_{1610}) [34]. The formula for calculating the degree of esterification (DE) is as follows:

$DE\% = A_{1740}/(A_{1740} + A_{1610}) \times 100\%$.

2.6 Monosaccharide composition

The method for monosaccharide analysis was based on a previously published protocol with slight modifications(Chen et al., 2021). To summarize, a 10 mg sample was solubilized in 4 mol/L TFA (10 mL), homogenized, and incubated for 3 h at 120 °C. Afterward, the reaction mixture was evaporated under nitrogen and methanol. The decomposed sample was resuspended in distilled water. An aliquot of this solution (400 μL) was then mixed with 0.3 mol/L NaOH solution (450 μL) and 0.3 mol/L PMP-methanol solution (450 μL), and the blend was heated at 70°C for 30 min. Once cooled, 0.3 mol/L HCl (450 μL) was introduced. The treated sample solution was extracted with chloroform to isolate the upper aqueous layer, which was then filtered through a 0.45 μm water membrane prior to injection. Each solution (10 μL) was analyzed using an HPLC system (Shimadzu, Kyoto, Japan) with a photodiode array detector and a C18 column (4.6 mm × 250 mm, 5 μm, Shimadzu, Kyoto, Japan). The chromatographic separation was conducted at 25 °C with a mobile phase comprising solvent A (15% v/v of 0.05 mol/L phosphate buffer in acetonitrile) and solvent B (40% v/v of 0.05 mol/L phosphate buffer in acetonitrile) at a flow rate of 1.0 mL/min. The gradient elution began at 0% solvent B, rising linearly to 15% over 10 min, then to 25% over the subsequent 20 min, and held at 25% for an additional 25 min. Detection was set at 250 nm wavelength.

2.7 Zeta potential and particle size analysis

The colloidal properties of LP fractions and yogurt samples were evaluated using a Zetasizer Pro (Malvern Instruments Ltd, Worcestershire, UK). For LP fractions, the zeta-potential was measured at 1 mg/mL in ultrapure water. For yogurt samples, 10 mg of yogurt was homogenized in 10 mL of deionized water via sequential vortex mixing (30 s, 700 × g) and ultrasonic processing (20 kHz, 3 times 10 s pulses at 50 W). The particle size in the fluid phase was determined by dynamic light scattering and is reported as the Z-average particle size based on the intensity distribution of scattered light. The refractive index was calibrated to 1.33. Both particle size and zeta-potential were determined via Dynamic Light Scattering (DLS).

Samples were allowed to equilibrate for 2 min before testing. The physical stability of the yogurt was monitored at 1, 7, and 14 days of storage under identical conditions. All measurements were conducted under ambient temperature conditions.

2.8 FT-IR spectral analysis

The Fourier transform infrared (FT-IR) spectroscopic analysis of the pectin samples was carried out using a Nicolet-iS5 spectrometer from Thermo Fisher Scientific, located in the United States. A 1.5 mg portion of the sample was combined with 198.5 mg of potassium bromide (KBr) and compacted into a tablet under a pressure of 25 MPa for a duration of 30 s. The spectral data were acquired over the wavenumber range extending from 4000 to 500 cm^{-1} with 32 scans per spectrum at a resolution of 4 cm^{-1}.

2.9 Apparent morphology

Pectin solutions at a concentration of 5 μg/mL were applied to newly cleaved mica surfaces and allowed to dry naturally at ambient temperature. Atomic force microscopy (AFM) was employed in the tapping mode to visualize the samples using a Dimension Icon instrument from Bruker, based in Rheinstetten, Germany. The microstructural analysis of the samples was performed using a scanning electron microscope (SEM), specifically a Merlin Compact model from Zeiss EVO/LS10, Germany. For SEM examination, LP samples weighing 2 mg were coated with a thin layer of gold and then attached to an aluminum stub, operating at a voltage of 5.0 kV.

2.10 Rheological measurements

The method for assessing the apparent viscosity and viscoelastic behavior of pectin samples was slightly modified [36]. Flow curves for the LP fractions (10 mg/mL, w/v) were generated at 25 °C on a rheometer (DHR-2, TA Instruments) using a C35 cone-plate (35 mm, 1.99°, 46 μm gap) across a shear rate (γ) range of 0.1 to 100 s^{-1}. The shear stress (τ) data were fitted to the Herschel-Bulkley model:

$\tau = \tau_0 + K\gamma^{n-1}$,

to determine the yield stress (τ_0), consistency index (K), and flow behavior index (n).

Additionally, the dynamic oscillatory properties of LP fractions were evaluated via frequency sweeps (0.1–100 rad/s) at 25 °C using the same cone-and-plate geometry to determine their storage modulus (G′), and loss modulus (G″).

Measurements for yogurt were conducted at 4 °C to maintain gel structural integrity. Steady-state flow behavior (apparent viscosity and shear stress) was measured over a shear rate range of 0.1 to 100 s^{-1} using a 40 mm parallel-plate geometry with a 1000 μm gap. Subsequently, the viscoelastic behavior of the yogurt matrix was assessed at 4 °C using the parallel-plate geometry (40 mm diameter, 1000 μm gap). Frequency sweeps were performed from 0.1 to 100 rad/s to quantify the storage modulus (G′), loss modulus (G″), and loss tangent (tan δ = G″/G′).

2.11 Thermal gravimetric analysis

The thermal and differential scanning calorimetric characteristics of the pectin samples were investigated using a TA Instruments Universal V4.5 A TGA, located in New Castle, USA. The samples were subjected to a temperature ramp from 27 °C to 600 °C at a uniform rate of 10 °C per minute in an atmosphere of dry nitrogen.

2.12 Antioxidant analysis

2.12.1 ABTS free radical scavenging activity

To determine the scavenging ability of the polysaccharides against $ABTS^{+}\bullet$ [37], 100 μL of the polysaccharide solution was mixed with 1 mL of an $ABTS\bullet^{+}$ working solution for 6 min. The $ABTS\bullet^{+}$ working solution was obtained by mixing a 7.4 mmol/L $ABTS^{+}\bullet$ solution and a 2.6 mmol/L $K_2S_2O_8$ solution and then incubating the mixture for 12–16 h. The solution was diluted with phosphate buffer (pH 7.4) to an absorbance value of 0.70 ± 0.02 at 734 nm. Vitamin C (Vc) served as the positive control, and the scavenging capacity was calculated using the following formula:

Scavenging ability (%) = $(1-(A_1+A_2)/A_0) \times 100\%$,

where A_0, A_1, and A_2 are the absorbances of the blank, sample or Vc, and control, respectively.

2.12.2 DPPH scavenging activity

To evaluate the scavenging potential of the samples on $DPPH^{+}$ [23], the polysaccharides at various concentrations were mixed with the same volume of a 0.2 mmol/L DPPH-ethanol solution. The absorbance at 517 nm was measured after 30 min of reaction in the dark.

2.12.3 Ferric-reducing antioxidant power (FRAP) test

To evaluate the reducing ability of the polysaccharides [38], The FRAP working solution comprised 25 mL of acetate buffer (pH 3.6), 2.5 mL of 10 mmol/L TPTZ solution, and 2.5 mL of 20 mmol/L $FeCl_3$. The sample supernatant (10 μL) was added to 190 μL of the working solution, followed by incubation at 37 ºC for 20 min. A spectrophotometer was used to measure the absorbance at 593 nm. Trolox was used as a positive control standard. The reducing power was calculated and expressed as micromoles of Trolox equivalent per gram of dry weight (μmol Trolox/g DW).

2.13 Preparation and characterization of lemon pectin yogurt (LPY)

2.13.1 Preparation of yogurt

Yogurt was prepared according to a published method [4] with minor modifications. Commercial whole milk (protein content 3.4 g/100 mL, fat content 3.5 g/100 mL) was used as the base. Briefly, milk supplemented with 0.5% (w/v) of LP20, LP40, LP60, or LP80 pectin powders was homogenized in glass bottles. The mixtures were sterilized at 85 °C for 30 min, then cooled to 43 °C. A commercial yogurt starter culture (a 1:1 mixture of *Streptococcus thermophilus* and *Lactobacillus delbrueckii subsp. bulgaricus*) was inoculated at 0.1% (w/v) into the cooled mixtures, followed by fermentation at 43°C for 6 h in a constant-temperature incubator until the pH reached 4.6. Control yogurt was prepared identically, without the addition of pectin. All samples were refrigerated overnight at 4 °C before analysis.

2.13.2 Water-holding capacity

The water-holding capacity was determined using the established centrifugation method [39]. Briefly, gel samples (10 ± 0.5 g) were centrifuged at 1,000 × g for 10 min at 4°C. The exudate was carefully removed with absorbent paper, and WHC was calculated using the equation:

$$WHC\ (\%) = (W_{initial} - W_{expelled}/W_{initial}) \times 100$$

Where $W_{expelled}$ represents the weight of expelled water, and $W_{initial}$ denotes the initial weight of the gel prior to centrifugation.

2.13.3 LPY strength measurement

The textural properties of homogenized yogurt systems, either without additives or supplemented with distinct LPY fractions, were measured using a texture analyzer (CT3, Brookfield, USA). A cylindrical probe (type P/0.5, 15 mm diameter) was used to penetrate yogurt samples (25 mm diameter, 20 mm height) under standardized conditions: a trigger force of 8 g, a constant penetration speed of 2 mm/s, and a target depth of 10 mm. Gel hardness was defined as the peak force during the first compression cycle. Gel strength was quantified as the maximum force (expressed in grams, g) recorded by the probe at the 10 mm penetration depth.

2.13.4 Microscope of LPY measurement

For microstructural characterization, 10 mg aliquots of distinct yogurt formulations were dispersed in 10 mL deionized water through sequential vortex mixing (30 s, 1,000 × g) and ultrasonication (20 kHz, 3 × 10 s pulses at 50 W) to achieve colloidal homogeneity. This sample preparation focuses on the size and morphology of primary protein-pectin aggregates rather than the intact three-dimensional gel network. The primary microstructure was examined using an optical microscope (Zeiss Primostar 3, Carl Zeiss (Suzhou) Co., Ltd., China) at 20 × magnification with phase-contrast illumination. Note that dispersion may alter the native network. Observations thus reflect dispersed microstructural features for comparative analysis, not the pristine gel structure.

2.13.5 Fluorescence microscopy measurement of LPY

Based on previous reports, the relationship between LP components and the dispersion of yogurt proteins was investigated with slight modifications [40]. A yogurt sample (0.2 g/mL) was mixed with an equal volume of rhodamine B (10 μg/mL) and incubated in the dark for 1 h. The sample was then washed twice with PBS until the supernatant became clear. The stained sample was observed under a fluorescence microscope (Eclipse Ti2-U; Nikon, Tokyo, Japan), with red areas indicating the protein phase stained by rhodamine B. Note that dispersion may alter the native network. Observations thus reflect dispersed microstructural features for comparative analysis, not the pristine gel structure.

2.13.6 Measurement of molecular interaction forces in LPY

Based on previous reports, the interaction between LP components and yogurt proteins was evaluated [41]. The following solvents were prepared: (i) S1, distilled water; (ii) S2, 0.086 mol/L Tris, 0.09 mol/L

glycine, and 4 mmol/L Na_2EDTA (pH = 8.0); (iii) S3, S2 supplemented with 0.5% SDS; (iv) S4, S3 with 8 mol/L urea; (v) S5, S4 with 2% β-mercaptoethanol. 500 mg of gel was thoroughly mixed with 10 mL of solvent and incubated in a water bath at 25 °C for 2 h. The mixtures were then centrifuged at 4,000 × g for 15 min. Protein content in the supernatant was quantified using the Bradford method. Protein solubility was expressed as the ratio of supernatant protein content to total protein content. Differences in solubility between S2 and S1 reflect electrostatic interactions; between S3 and S2, hydrophobic interactions; between S4 and S3, hydrogen bonding; and between S5 and S4, disulfide bonds. These chemical treatments, while selective, may not exclusively target single interactions in complex gels. Consequently, solubility changes reflect the relative contribution or network sensitivity to each condition, not absolute interaction energies.

2.14 Statistical analyses

Experiments were conducted with three independent biological replicates for the core fermentation and textural studies, with each replicate representing a separately prepared batch. Technical replicates were used only for specific analytical procedures, as noted in the relevant method descriptions. All data are expressed as mean ± standard deviation (SD). One-way ANOVA was performed using SPSS 26.0 software, and Duncan's multiple range test was used at a 5% confidence level.

3. Results and discussion

3.1 Physicochemical characteristics of LP fractions

Pectin was isolated from waste lemon peels by leveraging the differential ethanol solubility of pectin with distinct MW and lyophilized samples were successfully obtained, confirming the feasibility of this strategy (**Figure 2A**). The yield and purity of the isolated LP fractions were subsequently analyzed (**Table S1**). The yields were ranked as follows: LP40 (38.64%) > LP60 (25.75%) > LP20 (18.81%) > LP80 (12.23%), while the maximum protein and polyphenol contents were 0.38% (w/w, LP20) and 0.54% (w/w, LP20), respectively. Furthermore, the weak UV absorbance of the LP fractions at 260 nm and 280 nm indicated minimal nucleic acid and protein contamination [27] (**Figure S3**). Notably, all LP fractions exhibited total sugar contents exceeding 85%, with acidic sugar contents of LP40 and LP60 surpassing 60%, meeting commercial pectin standards. These results demonstrate that the solubility-based separation method achieves high efficiency and purity.

MW is the most critical physicochemical parameter of polysaccharides, typically determining their bioactivity and gelling properties. As shown in **Figure 2B** and **Table S1**, the MW of the four fractions were determined as: LP20 (45.33 kDa) > LP40 (40.09 kDa) > LP60 (20.01 kDa) > LP80 (7.77 kDa). This data confirms the method's efficacy in separating pectin fractions by MW and demonstrates significant differences among LP fractions. Moreover, LP fractions exhibited the narrowest MW distribution (1.15-1.86), which may contribute to the formation of its homogeneous (**Table S1**). Furthermore, since particle size is closely related to polysaccharide MW [42,43]. The Z-average particle size distribution of the pectin fractions, which significantly decreases as the ethanol precipitation concentration increases. The observed particle size

dropped from approximately 811.5 nm for LP20 to 334.15 nm for LP80. This trend is highly consistent with the descending order of MW shown in Figure 2B (from 45.33 kDa to 7.77 kDa), providing strong evidence for the positive correlation between particle size and the MW of polysaccharides (**Figure 2C**). Collectively, LP fractions exhibit distinct MW and particle sizes.

Polysaccharides possess diverse functional groups, the variations of which can be utilized for polysaccharide classification and characterization of their gel properties. As shown in **Figure S4**, FTIR spectroscopy revealed distinct functional groups in LP fractions. Typically, the broad and intense peak observed around 3429 cm^{-1} in all four pectin samples corresponds to O-H stretching vibrations, characteristic of polysaccharides [44]. Absorption bands at 1727 cm^{-1} and 1610 cm^{-1} indicate C=O stretching vibrations of esters and asymmetric stretching of COO-, respectively, confirming the presence of uronic acids in all LP fractions [45,46]. FTIR spectroscopy revealed that LP20, LP40, and LP60 exhibited esterification degrees >50% with no significant differences among them, whereas LP80 showed <50% esterification (**Figure 2D**), classifying LP20-LP60 as high-methoxyl pectin and LP80 as low-methoxyl pectin. Previous studies have demonstrated that low-esterified pectin, exposing more carboxyl groups, can form superior "egg-box" gels through Ca^{2+} crosslinking [47]. Furthermore, absorption peaks between 1200-800 cm^{-1} represent the polysaccharide "fingerprint region", with 1076 cm^{-1} indicating pyranose and 895 cm^{-1} corresponding to β-pyranose [48,49]. These results demonstrate that LP fractions share similar functional group profiles, suggesting ethanol precipitation preserves the native glycosidic bond types in pectin.

Zeta potential measurements showed values of -19.13 mV (LP20), -17.69 mV (LP40), and -12.78 mV (LP60), contrasting with -22.98 mV for LP80 **(Figure 2E**). The universal negative charges originate from galacturonic acid residues[50]. Intriguingly, LP80 with the lowest esterification degree (30.13%) displayed the highest absolute potential (-22.98 mV). However, the expected correlation between decreasing esterification and increasing potential magnitude was absent in LP20-LP60, suggesting structural determinants beyond simple charge density. We propose two potential mechanisms: (i) molecular conformation may affect charge exposure, where larger molecules could extend more effectively. (ii) interfacial steric effects from varying adsorbed layer thickness could alter the slipping plane position. Thus, zeta potential reflects combined effects of charge density, conformation, and interfacial structure.

Monosaccharide composition analysis elucidates the primary structure of pectin[51]. As shown in **Table S2** and **Figure S5**, all LP fractions comprised seven monosaccharides: mannose (Man), rhamnose (Rha), galacturonic acid (GalA), glucose (Glc), galactose (Gal), arabinose (Ara), and fucose (Fuc). Despite variations in monosaccharide ratios, all LP fractions shared identical sugar species. GalA dominated the composition (>60%), with Gal, Ara and Rha being the major neutral sugars. Notably, homogalacturonan (HG) constituted >50% of all LP fractions, peaking at 68.12% in LP20. The zeta potential trends of LP20-LP60 correlated with HG content (**Figure S6**). It is important to note that these key structural parameters, Mw, DE, and HG content, naturally co-vary across the fractions. The observed co-variation of Mw with DE and HG content provided a rigorous test for our hypothesis. It allowed us to determine whether Mw could predict

texture across a naturally occurring spectrum of pectin structures, thereby assessing its real-world utility as a design parameter. Collectively, as schematized in **Figure 2F**, the LP fractions exhibit similar primary structures, and our results establish molecular weight as the primary control variable that dictates the transition of interaction forces in the yogurt matrix.

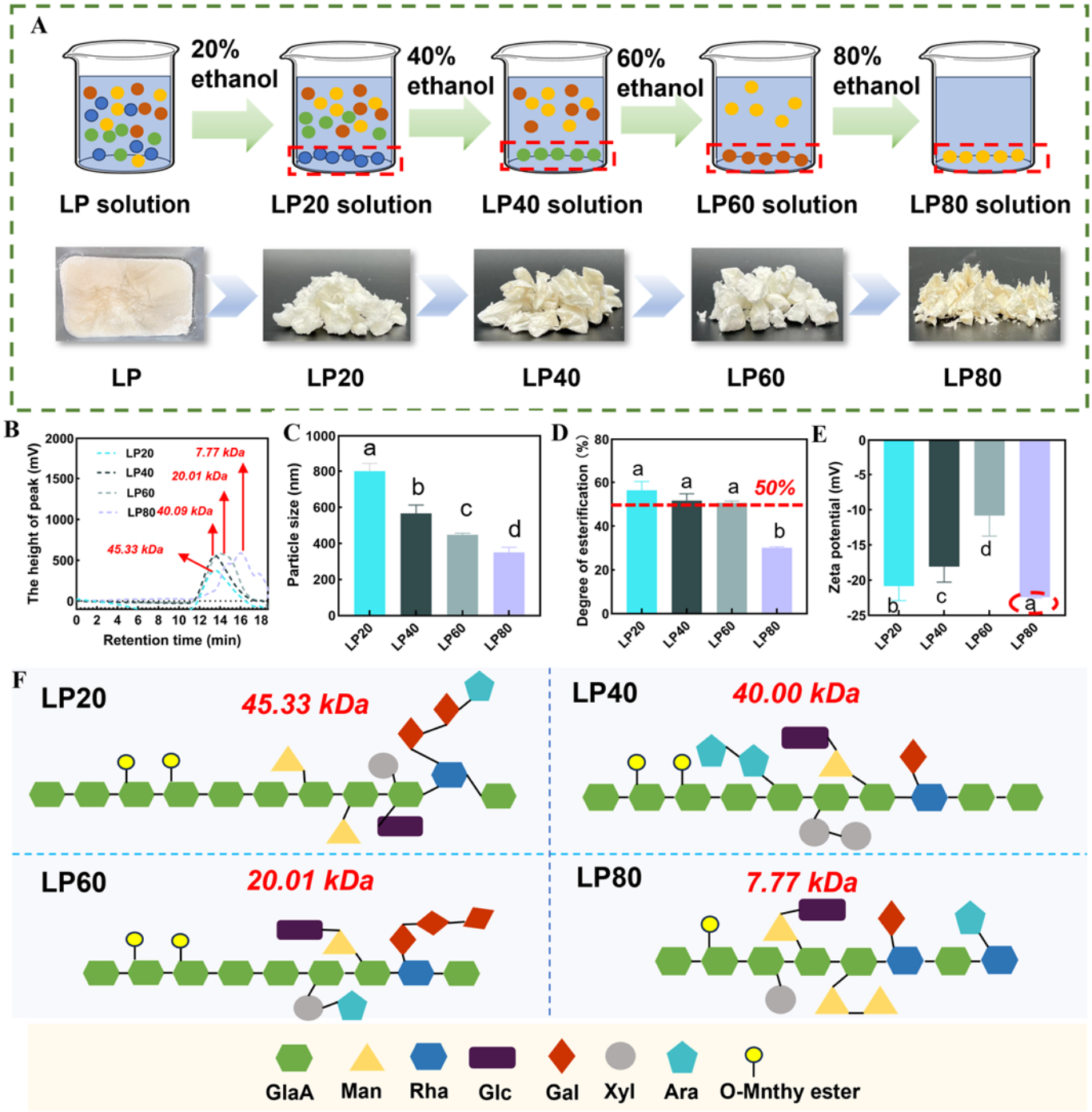

Figure 2. Isolation and physicochemical characterization of lemon pectin (LP) fractions. (**A**) Schematic of molecular weight (MW)-based LP fractionation using a sequential ethanol gradient precipitation (20%–80%, v/v). (**B**) MW distribution profiles of LP fractions determined by HPLC-GPC; peaks are labeled with their respective weight-average MW. (**C**) Particle size distributions, expressed as the z-average hydrodynamic diameter (Dz), measured by Dynamic Light Scattering (DLS). (**D**) Degree of esterification (DE) quantified by FT-IR; the red dashed line at 50% distinguishes between high-methoxyl pectin (HMP, DE > 50%) and low-methoxyl pectin (LMP, DE < 50%). (**E**) Zeta potential measurements at pH 7.0, representing the surface net charge density. (F) Schematic structural model illustrating the MW-dependent variations in monosaccharide composition and esterification patterns. Data are presented as mean ± SD (n = 3). Different lowercase letters (a–d) within each panel indicate significant differences ($P < 0.05$) based on one-way ANOVA followed by Duncan's multiple range test.

3.2 Structure and function characteristics of LP fractions

The conformation of polysaccharides is generally categorized as being spherical, helical, rod-shaped, or irregularly coiled [52]. Red-shift in λmax indicates Congo red-polysaccharide triple-helix formation. The decrease in λmax at NaOH concentrations > 0.19 mol/L signifies the transition to random coil structures following hydrogen bond cleavage [53,54]. **Figure 3A** demonstrates that the maximum absorption peaks of LP pectin-Congo red complexes in NaOH (0-0.5 mol/L) systems remained lower than that of free Congo red, with no significant red shift observed. This observation indicates the absence of tertiary helical structures in LP pectin components.

The microscopic and surface morphology of LP fractions were observed by SEM. As illustrated in **Figure 3B**, all LP samples exhibited irregular surface architectures under low-magnification SEM. Specifically, LP20 showed a multi-layered, stacked morphology **(Figure 3B1**), whereas LP80 displayed a more exfoliated, flake-like structure (**Figure 3B4)**. The suggests that ethanol fractionation promotes structural disintegration from aggregated multilayers toward isolated fragments. Higher-magnification images revealed that these coarse features arose from the folding and aggregation of sheet-like substructures, particularly evident in LP20 and LP40 (**Figure 3B1–B2**), indicating that higher MW facilitates the formation of dense multilayer aggregates [55]. AFM topography images provided complementary insight into surface roughness and nanoscale organization (**Figure 3C**). LP20 exhibited a network of interwoven linear structures with uniform layer distribution (**Figure 3C1**), a morphology potentially conducive to enhanced viscosity[56]. In contrast, LP40 showed granular features with limited branching (**Figure 3C2**), and both LP60 and LP80 displayed increased aggregation (**Figure 3C3** and **3C4**) [57]. The measured average roughness (Ra) values were 0.234 nm (LP20), 0.184 nm (LP40), 0.276 nm (LP60), and 0.228 nm (LP80) (**Figure S7**). Variations in Ra reflect the MW-dependent organizational tendencies of pectin fractions, where chain flexibility and entanglement dictate the transition from tight molecular packing in LP40 to the aggregation of high-surface-energy species in LP60 and LP80.

The variation in MW of pectin is typically accompanied by shifts in physicochemical properties and biological activities, which indirectly influence the sensory and nutritional value of yogurt. As shown in **Figure 3D**, initial viscosity followed the order of LP20 > LP40 > LP60 > LP80, with all LP fractions exhibiting shear-thinning behavior (measured at a shear rate of 0.1 s^{-1}), indicating a clear positive correlation between viscosity and MW. Rheological analysis revealed that all LP fractions exhibited near-Newtonian flow behavior (flow index n ≈ 11, negligible yield stress) according to the Herschel-Bulkley model (R^2 > 0.98), with the consistency index (K) of LP20 being an order of magnitude higher than the other fractions (**Table S3** and **Figure S8**) [58]. TGA analysis identified a three-stage thermal degradation profile (**Figure 3E** and **Table S3**), where initial hydration capacities (mass loss: 4.86%–18.72%) displayed a clear MW dependency [59,60]. As ethanol fractionation progressed, the maximum decomposition temperatures during pyrolysis increased significantly; notably, LP80 demonstrated superior thermal resistance and enthalpy changes (ΔH_d), suggesting that a hydrogen-bond-stabilized structural network enhances its overall integrity

[61]. The antioxidant capacity of LP fractions exhibited a consistent MW-dependent trend across all assays (**Figure S9**). In ABTS assays (**Figure S9A**), the scavenging efficacy at 4 mg/mL followed the order: LP80 (78.23%) > LP60 (63.12%) > LP40 (58.89%) > LP20 (42.54%). Consistently, ferric reducing power analysis showed that LP80 (0.98 mV) significantly outperformed LP20 (0.45 mV) (**Figure S9B**). DPPH assays further confirmed this pattern, with LP80 exhibiting the highest activity (58.66%) and LP20 the lowest (38.10%) (**Figure S9C**). These results indicate that lower-MW fractions possess superior antioxidant potential due to their enriched reducing sugar content. The standardized heatmap reveals a functional divergence where LP20 dominates rheological parameters, while LP80 excels in antioxidant capacity (**Figure 3F**). This distinct "structural-bioactive" trade-off suggests that selecting specific LP fractions will differentially impact yogurt quality, modulating either textural thickness or nutritional stability.

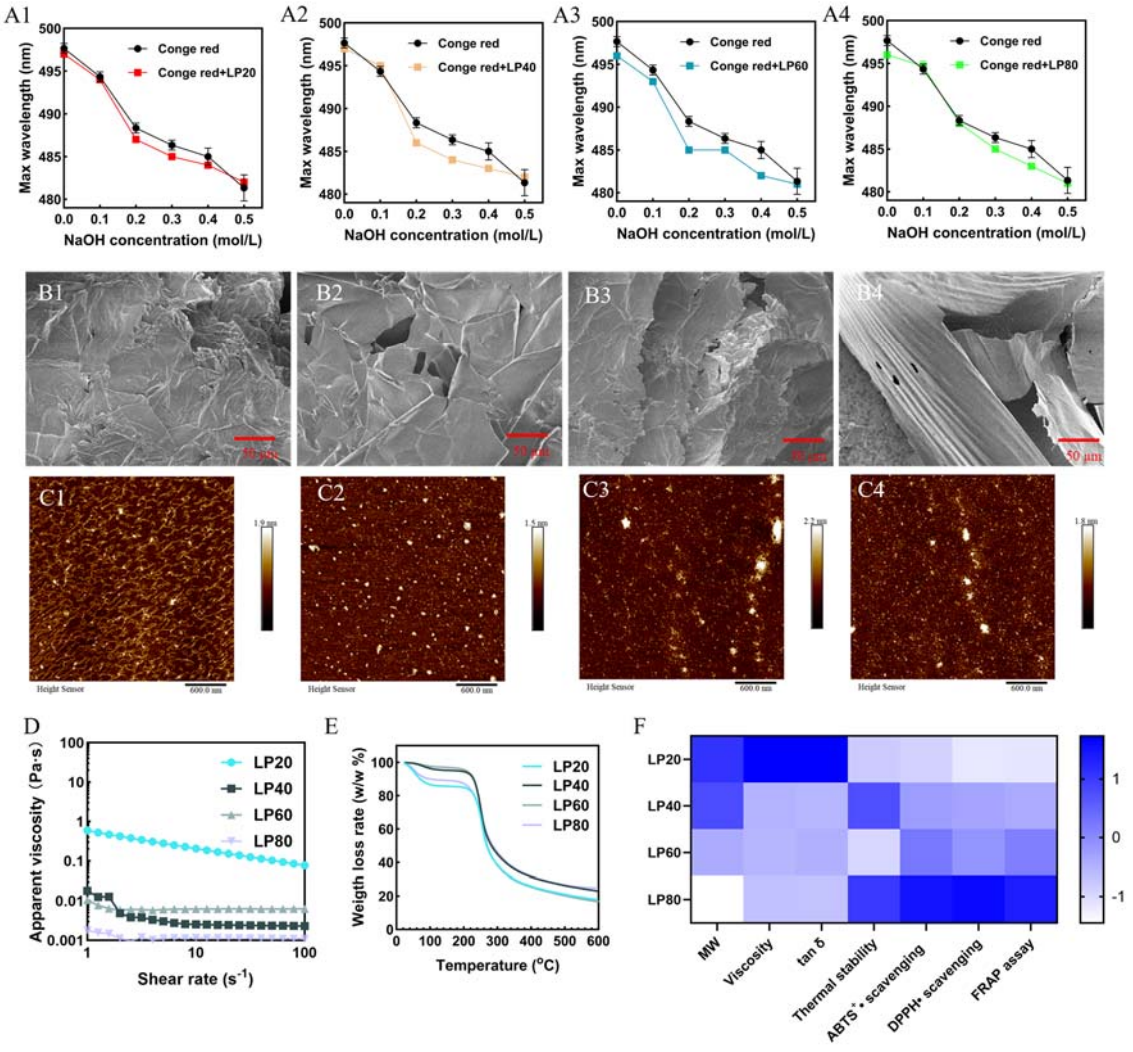

Figure 3. Morphological architectures, physicochemical properties, and structure-function correlations of LP fractions. (**A1-A4**) Congo red assays illustrating the triple-helix conformational stability of LP fractions under varying NaOH concentrations, (**B1-B4**) Scanning electron microscopy (SEM) images revealing the surface topography of LP fractions at 500 × magnification (scale bars = 50 μm). (**C1–C4**) Atomic force microscopy (AFM) height images (2D) showcasing the chain aggregation and molecular height distribution (scale bars = 600 nm). (**D**) Apparent viscosity (Pa·s) as a function of shear rate (s^{-1}) at 25 °C, demonstrating the non-Newtonian flow behavior of the fractions. (**E**) Thermogravimetric (TG) thermograms showing the weight loss rate (w/w %) from 27 °C to 600 °C to evaluate thermal degradation stability. (**F**) Standardized Heatmap illustrating the integrated correlations between MW, rheological parameters (viscosity), thermal stability, and multi-faceted antioxidant activities ($ABTS^{+}$•, DPPH•, and FRAP assays); the color scale from blue to white represents standardized Z-scores from high to low.

3.3 Effects of LP components on yogurt

The incorporation of pectin effectively improves its textural properties. As a natural soluble dietary fiber, pectin also confers multiple health benefits, including gut health regulation and blood glucose control [62,63]. The final pH of all yogurt samples was tightly controlled, ranging from 4.55 to 4.65 (**Table S4**), confirming a uniform fermentation endpoint prior to texture and rheological analysis (**Figure 4)**. **Figure 4A** illustrates the preparation protocol of five yogurt formulations: one LP-free control group and four experimental groups supplemented with distinct LP fractions (LP20, LP40, LP60, LP80). Microscopic analysis (**Figure 4B**) revealed distinct structural organizations: controls displayed viscous fluidity, whereas the addition of LP20 caused visible whey separation (synersis), likely due to macromolecular exclusion-induced osmotic imbalance [64,65]. Notably, LP40 and LP80 formed continuous gels, whereas LP60 maintained homogeneous non-gel states, potentially through facilitating globular protein assembly [4]. Quantitative texture analysis revealed distinctive rheological modifications imparted by different LP fractions (**Figure 4C-F**). Both LP80Y and LP40Y significantly enhanced hardness, springiness, and chewiness ($P < 0.05$), forming elastic gels with multilayered mouthfeel characteristics. In contrast, LP60Y maintained native hardness while optimizing springiness and cohesiveness with reduced chewiness, resulting in rapid melt-in-mouth properties particularly suitable for dysphagia diets. Although LP20Y exhibited syneresis-mediated reduction in hardness and cohesiveness, it developed unique textural complexity through elevated chewiness and springiness. Critically, the observed syneresis in LP20Y led to a reduction in its macro-stability, which suggests that excessively high Mw may disrupt the optimal arrangement of the casein network [66]. These differential effects originate from MW-dependent pectin-casein interactions.

Yogurt stability, a crucial parameter determining shelf life and consumer acceptance, was systematically investigated through zeta potential analysis [67]. Initial fermentation yielded more negative potentials in control (-13.8 mV) and LP20Y (-16.2 mV) samples, attributable to charge superposition between casein and pectin (**Figure 4G**). Throughout storage (**Figures 4H-I**), control and LP20Y exhibited substantial potential reduction within 7 days with progressive drift over 14 days, whereas LP40Y, LP60Y and LP80Y maintained remarkable stability ($\Delta < 5$ mV). Comparative analysis demonstrated 80% potential variation in control, significantly surpassing the <50% change observed in LP-modified samples (**Figure 4J**). Particularly, LP40Y and LP80Y showed minimal drift (<5%), while LP60Y displayed intermediate stability (∼10%). Notably, stability enhancement relative to control followed the order: LP80 (12.0-fold) > LP40 (10.1-fold) > LP60 (8.6-fold) > LP20 (1.6-fold). These results reveal how lower-Mw pectin fractions achieve superior stabilization through efficient adsorption on casein micelles, whereas the longest chains (LP20) fail to stabilize the network due to bridging flocculation or depletion effects. This is a key insight for developing consumer-friendly yogurts with extended shelf life.

Building on the finding that pectin functionality is closely linked to its MW, we propose a novel strategy: the targeted use of specific pectin fractions could be developed into a reliable method for designing yogurt with customizable stability and textural profiles (**Figure 4K**). Consistent with the rheological and syneresis

results presented above, the microstructure analysis revealed a clear non-monotonic relationship between pectin MW and gel network integrity (**Table S1)**. Rheological characterization revealed a systematic MW-texture gradient, with LP60Y exhibiting low chewiness/high cohesiveness, a combination of textural parameters that aligns with the rheological criteria often recommended for dysphagia diets, while LP40Y and LP80Y displayed contrasting high chewiness/low cohesiveness profiles. Fundamentally, MW governs the primary texture formation mode, while secondary structural parameters such as degree of esterification fine-tune texture intensity within each mode. Although LP40 and LP80 differ substantially in esterification degree, both generated solid gels through distinct mechanisms. The exceptional gel strength of LP80Y reveals a unique synergistic mechanism, low MW enables efficient cross-linking and dense integration within the casein network. Simultaneously, its reduced esterification exposes additional carboxyl groups. These groups enhance both hydrogen bonding and calcium-mediated bridging, even under acidic yogurt conditions. This cooperative interaction produces a uniquely reinforced yet homogeneous gel architecture (**Table S1**). It is important to note that the indicated suitability of LP60Y for dysphagia management is based on instrumental texture and rheological profiles matching theoretical guidelines. Its practical efficacy and acceptability for target populations require future validation through clinical studies and sensory evaluation.

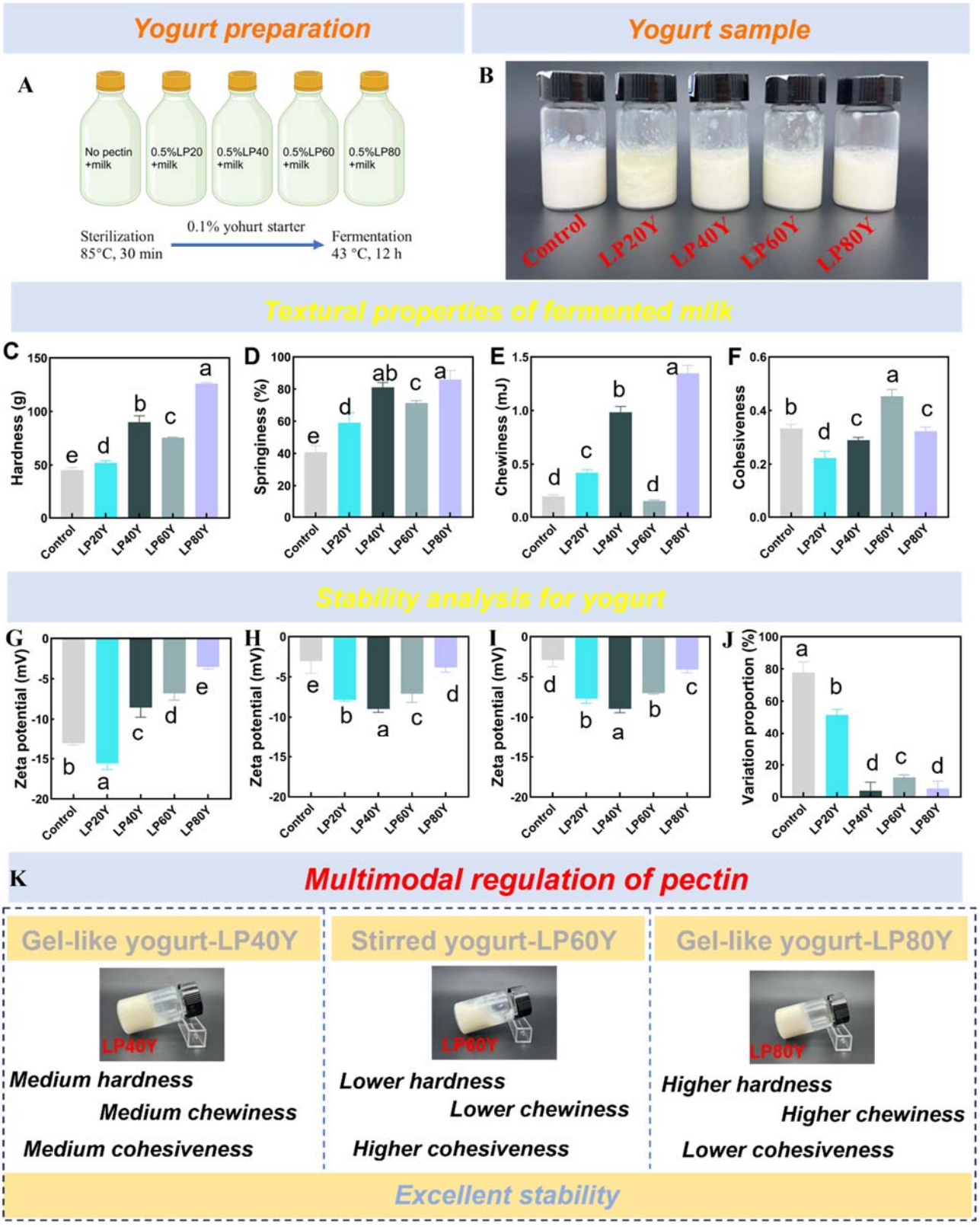

Figure 4. Multimodal yogurt modulation by LP fractions of distinct molecular weights. (**A**) Schematic representation of the yogurt fermentation process supplemented with 0.5% (w/v) LP fractions. (**B**) Visual appearance of final yogurt products: Control (pectin-free), LP20Y, LP40Y, LP60Y, and LP80Y, prepared using pectin with MW of 45.33, 40.09, 20.01, and 7.77 kDa, respectively. (**C–F**) Textural profile analysis of yogurt samples: (**C**) Hardness (peak force during the first compression, g), (**D**) Springiness (ability to recover after deformation, %), (**E**) Chewiness (work required to masticate the sample, mJ), and (**F**) Cohesiveness (ratio of the second to first compression area). (**G–I**) Long-term stability assessment via zeta-potential measurements monitored at (**G**) Day 1, (**H**) Day 7, and (**I**) Day 14 of storage at 4 °C. (**J**) Variation proportion (%) representing the relative percentage change in zeta-potential after 14 days to evaluate electrostatic stability. (**K**) Physical appearance and phase separation of yogurts texture. Data are expressed as mean ± SD (n = 3). Different lowercase letters within each panel indicate significant differences ($P < 0.05$) among groups as determined by Duncan's multiple range test.

3.4 Physical properties of yogurt

The particle size distribution directly reflects the dynamics of protein-polysaccharide interactions in yogurt [68]. While LP20Y showed a negligible impact on particle size compared to the control (**Figure 5A**), it induced pronounced phase separation, reflecting a physically unstable system (**Figure 4B**). This apparent contradiction suggests a mechanism dominated by depletion flocculation; the ultra-high-MW chains of LP20 are excluded from the inter-particle space of casein micelles, creating an osmotic pressure gradient that drives rapid, unstable aggregation into a heterogeneous network without significantly altering primary aggregate size [69]. In contrast, LP60Y and LP80Y significantly reduced the average particle size, while LP40Y resulted in a slight yet statistically significant reduction. This trend indicates that lower-MW chains, characterized by higher molecular mobility and reduced steric hindrance, can penetrate the casein matrix more effectively to coat protein surfaces. This uniform coating provides superior electrosteric stabilization, effectively limiting uncontrolled protein-protein aggregation during fermentation. Diverging from established reports of larger aggregates in low-ester pectin (DE<50%), LP80Y unexpectedly exhibited smaller particle sizes [70,71]. These findings conclusively establish MW, rather than esterification degree, as the dominant determinant of particle size in this system, as the physical constraints of short-chain length override the chemical propensity for calcium-induced cross-linking.

Water-holding capacity analysis revealed significantly improved water retention in all samples except LP20Y, which exhibited the lowest WHC due to the heterogeneous network (**Figure 5B**). The reduced WHC and severe syneresis in LP20Y are primarily attributed to depletion flocculation induced by its high MW. The large pectin chains are excluded from the volume surrounding casein micelles, creating an osmotic pressure that drives the micelles into dense, heterogeneous aggregates prone to whey expulsion. Within this dominant depletion framework, strong local pectin, casein interactions, possibly mediated by hydrogen bonding or electrostatic attraction, may further promote inhomogeneous aggregation and thus contribute to network instability [72]. LP80Y exhibited the highest WHC (82.45%), representing a 1.39-fold increase over the control. Both LP40Y and LP60Y also showed significantly higher water-holding capacity (70.56% and 72.13%, representing 1.31-fold and 1.24-fold increases, respectively) compared to the control, although no significant difference was observed between these two groups. Viscosity profiles demonstrated substantially higher initial viscosities in LP-fortified yogurts (**Figure 5C**). All formulations displayed characteristic shear-thinning behavior, consistent with shear-induced disruption of pectin-protein networks. As summarized in **Table S5**, the consistency index (***K***), showed a pronounced dependence on MW: LP40Y (32.0 $Pa \cdot s^n$) > LP60Y (18.3 $Pa \cdot s^n$) > LP80Y (8.46 $Pa \cdot s^n$). This inverse relationship suggests that, within this concentration regime, shorter pectin chains (higher yield fractions like LP40Y) contribute more effectively to the formation of a dense, viscous network, thereby serving as the dominant control variable for textural and organoleptic modification.

Rheological characterization via small-amplitude oscillatory shear revealed that all yogurt samples exhibited typical weak gel behavior, with the storage modulus (G′) consistently surpassing the loss modulus

(G″) across the measured frequency range (1–100 rad/s). The incorporation of LP fractions significantly enhanced the viscoelasticity of yogurt, as evidenced by the markedly higher G′ and G″ values of all LP-fortified yogurts compared to the control (**Figure 5D-5H**). The loss factor (tan δ = G″/G′) served as a key indicator of gel strength [73]. LP40Y (tan δ = 0.22) and LP80Y (tan δ = 0.19) formed strong gels characteristic of set-style yogurt, whereas LP60Y (tan δ = 0.35) produced weaker gels typical of stirred-style yogurt, as its specific Mw inhibits large-scale casein aggregation (**Figure 5I**). Crucially, while LP20Y exhibited the highest moduli, this does not represent true structural strengthening; rather, it reflects the mechanical resistance of a collapsed, compacted protein matrix caused by severe phase separation. The enhanced viscoelasticity and variable gel strength induced by the LP fractions suggest that pectin MW modulates the electrostatic and hydrophobic interaction-driven assembly of a casein-pectin composite network, ultimately enabling the precise customization of yogurt texture.

Optical microscopy confirmed enhanced microstructural homogeneity, correlating with improved colloidal stability [74]. Optical microscopy revealed that the incorporation of LP components shifted yogurt from a heterogeneous to a homogeneous state. The transition from LP20Y to LP60Y visualized a systematic reduction in aggregate size, correlating with improved colloidal stability through enhanced particle dispersion: (i) from LP20Y to LP60Y, yogurt particles gradually decreased in size and became more uniform (**Figure 5J2-5J4**); (ii) While both the Control and LP80Y exhibited large protein aggregates, the nature of these aggregates was fundamentally different. The aggregates in the Control were coarse, disconnected, and prone to collapse, leading to syneresis. In contrast, LP80Y formed a continuous, space-filling network where the aggregates were firmly cross-linked, likely by the low-Mw, low-DE pectin, resulting in a rigid, stable gel (**Figure 5J1 and 5J5**). Further analysis of protein aggregation via protein localization showed that LP20Y exhibited a higher degree of protein aggregation, likely due to disordered rearrangement of casein induced by high-molecular-weight pectin, which also accounts for the observed whey separation in this group (**Figure 5K**). Both LP40Y and LP60Y displayed homogeneous protein distributions, suggesting that such uniformity may contribute to enhanced stability. It is noteworthy that LP60Y also exhibited finer particles and linear structures, distinct from those of other groups, leading to the inference that LP60 inhibits casein aggregation, resulting in a stirred-yogurt (liquid) consistency[75]. LP80Y exhibited strong, uniform fluorescence, indicating that low-MW pectin promotes a highly ordered, space-filling assembly of casein micelles. In conclusion, the MW of LP components modulates the size and dispersion state of yogurt protein particles, thereby influencing the textural properties of yogurt.

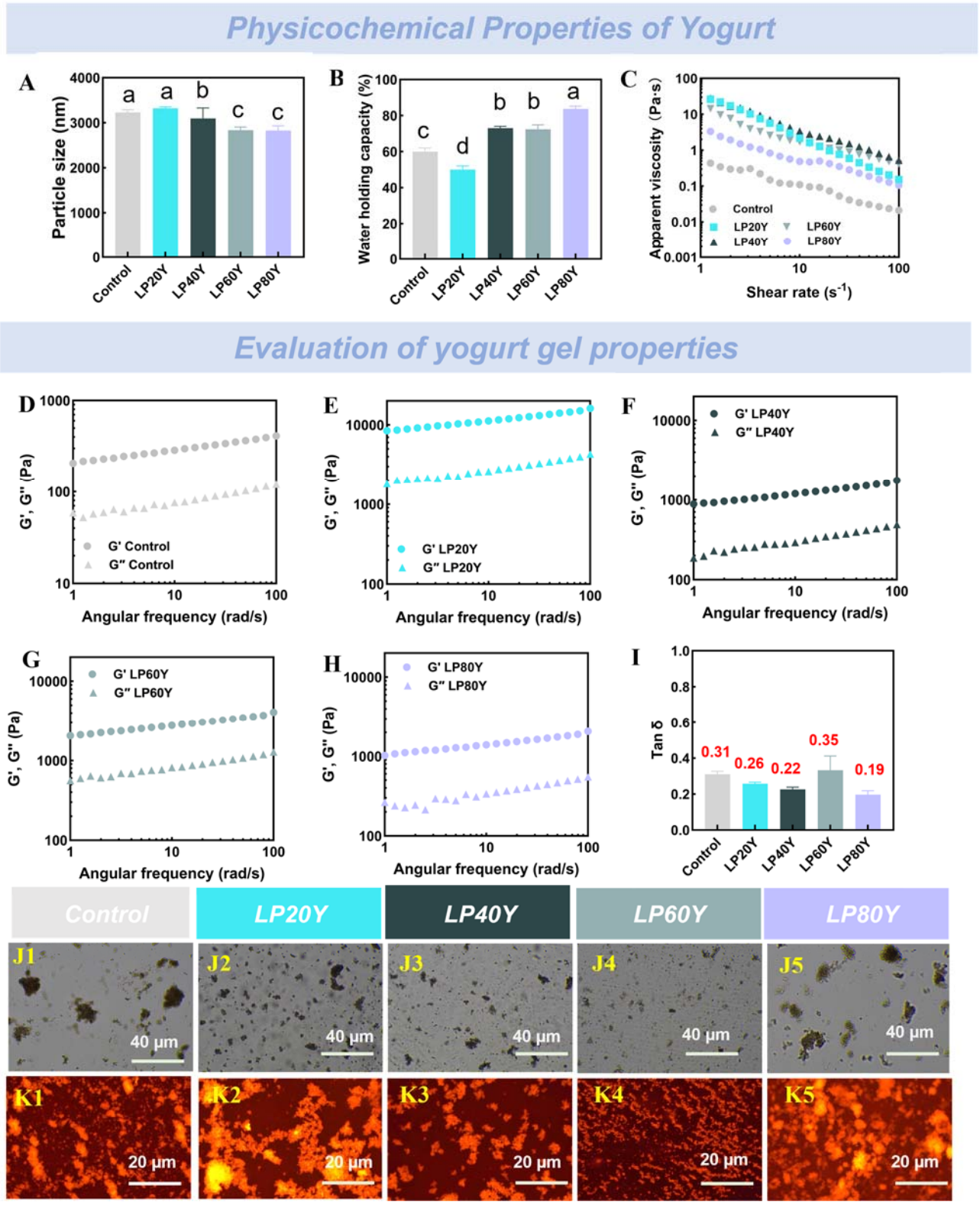

Figure 5. Physicochemical and microstructural characterization of yogurt modified with LP fractions. (**A**) Particle size distribution of yogurt samples, defined as the z-average hydrodynamic diameter (Dz), measured by DLS. (**B**) Water-holding capacity (WHC, %) representing the gel's ability to retain the aqueous phase under centrifugal force. (C) Apparent viscosity (Pa·s) at 4 °C, demonstrating shear-thinning behavior. (**D–H**) Dynamic oscillatory frequency sweeps (1–100 rad/s) at 4 °C illustrating the storage modulus (G′, Pa) and loss modulus (G″, Pa) for: (**D**) Control, (**E**) LP20Y, (**F**) LP40Y, (**G**) LP60Y, and (**H**) LP80Y. (**I**) Loss factor (tan δ = G″/G′) calculated at an angular frequency of 1 rad/s; values < 1 indicate dominant elastic (gel-like) behavior. (**J1–J5**) Optical micrographs (scale bars = 40 μm) visualizing the morphology of dispersed protein-pectin aggregates. (**K1–K5**) Fluorescence microscopy images (scale bars = 20 μm) with protein phases stained by Rhodamine B (red fluorescence); imaging was evaluated the spatial distribution of the protein matrix. Data are presented as mean ± SD (n = 3). Means labeled with different lowercase letters (a–d) within each panel differ significantly ($P < 0.05$) according to one-way ANOVA with Duncan's multiple range test.

3.5 The formation mechanism of the yogurt

The physicochemical properties of yogurt are closely correlated with the structure of polysaccharides [76]. To elucidate the effects of LP with different MW on the properties of yogurt (LPY), we further investigated the polysaccharide–protein and protein–protein interactions within the yogurt system (**Figure 6**). **Figure 6A** illustrates the structural similarity and distinct MW of LP, along with a schematic representation of their interactions with major milk proteins (casein and whey protein). Previous studies have shown that casein–polysaccharide interactions are influenced by electrostatic interactions, hydrogen bonding, and hydrophobic effects, while casein–whey protein interactions are strongly associated with disulfide bonds (**Figure 6B**). As shown in **Figure 6C–6F**, LP interactions with proteins were primarily mediated by electrostatic forces, hydrophobic interactions, and disulfide bonds, while hydrogen bonding played a secondary role. However, the impact of these interactions on the physical state of the yogurt is highly dependent on the pectin MW. It has been reported that while electrostatic interactions can support stable gel formation, an imbalance of these forces, particularly an excess of hydrophobic interactions in ultra-high MW samples like LP20Y, can promote protein over-aggregation and network collapse, leading to the macro-phase separation observed in the photographs. In contrast, the enhanced contribution of disulfide bonds in LP40Y and LP80Y serves as a critical covalent stabilizing factor, facilitating a robust and homogeneous solid gel network. In our study, LP40Y and LP80Y were highly dependent on disulfide bonds, which stabilized the gel network. This suggests that low-MW pectin effectively "unmasks" protein reactive sites or reduces steric barriers, facilitating covalent cross-linking between casein and whey proteins. In contrast, the stirred-yogurt characteristic of LP60Y was more reliant on electrostatic and hydrophobic interactions that maintained a balanced repulsion-attraction state, preventing rigid gelation. Based on these findings, we propose a four-phase MW-dependent regulation model (**Figure 6G**): (i) Ultra-high-MW pectin may trigger excessive aggregation and phase separation via strong depletion flocculation effects, leading to a physically unstable network and severe syneresis; (ii) High-MW pectin forms a continuous gel matrix via its backbone structure, effectively binding casein and whey protein to establish a stable solid gel; (iii) Medium-MW pectin co-assembles with proteins into a cohesive but flowable framework where balanced interactions contribute to a smooth, liquid-like yogurt texture; (iv) Low-MW pectin incorporates as fine particles within the casein–whey protein network, enhancing protein–protein interactions (particularly disulfide bonds) and modifying gel microstructure.

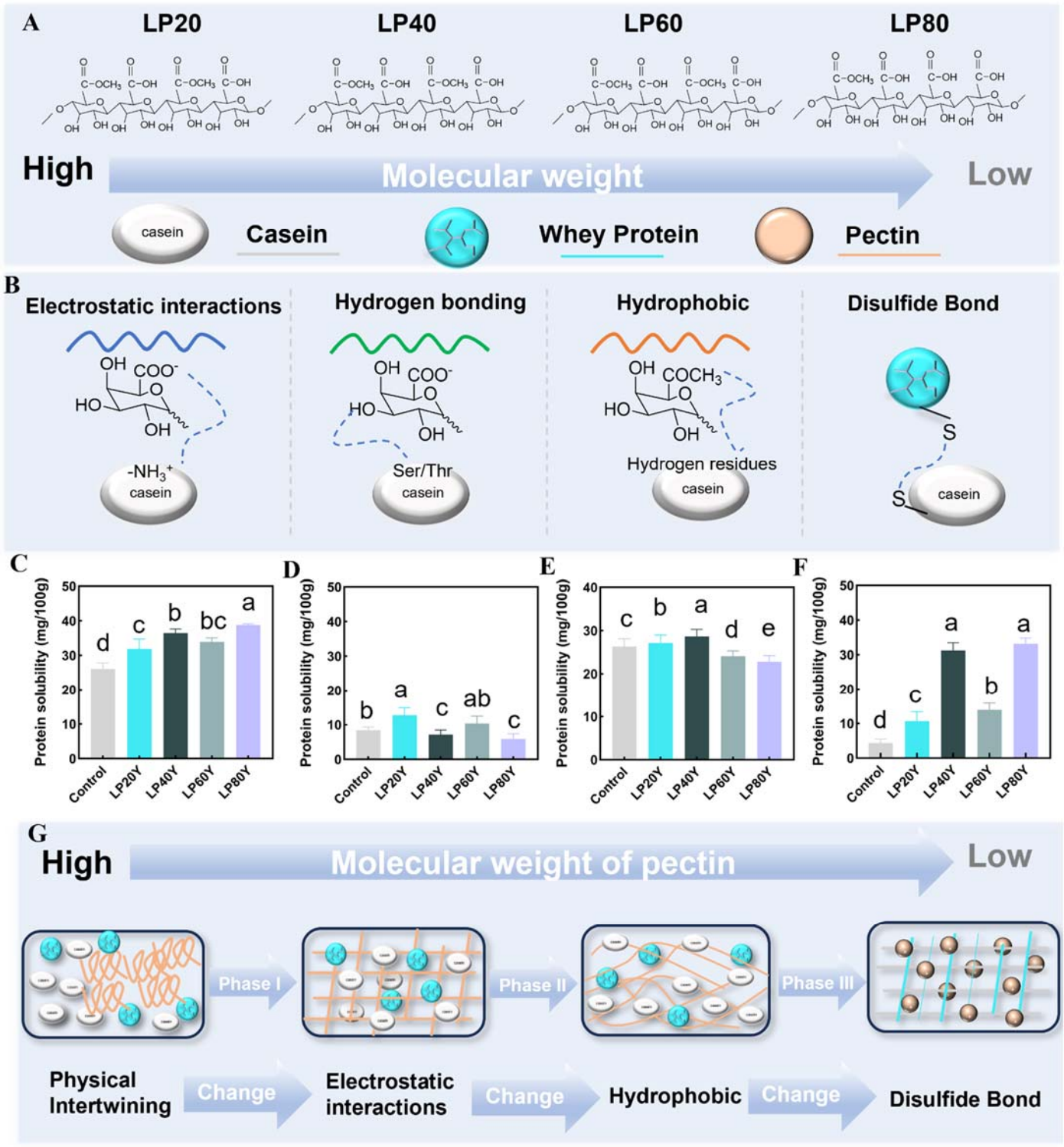

Figure 6. **Analysis of the molecular interaction forces between pectin and yogurt protein.** (**A**) Chemical structures and MW variations of LP fractions (LP20 to LP80), accompanied by a schematic legend for pectin and primary milk proteins (casein and whey protein). (**B**) Schematic illustrations of four key non-covalent and covalent interactions: electrostatic attractions, hydrogen bonding, hydrophobic effects, and disulfide linkages. (**C–F**) Quantification of relative interaction strengths in different yogurt matrices based on differential protein solubility in selective dissociating buffers: (**C**) Electrostatic interactions (solubility difference between S2 and S1); (**D**) Hydrogen bonding (solubility difference between S4 and S3); (**E**) Hydrophobic interactions (solubility difference between S3 and S2); and (**F**) Disulfide bonds (solubility difference between S5 and S4). Bar heights reflect the sensitivity of the protein network to each disruptive agent, representing the relative importance of that interaction to gel integrity. (**G**) Unified structural model illustrating the MW-dependent "multimodal" regulation mechanism, transitioning from physical intertwining to specific chemical bonding as pectin chain length decreases. Data are expressed as mean ± SD (n = 3). Different lowercase letters (a–e) indicate significant differences ($P < 0.05$) among groups.

4. Conclusion

This study establishes that the molecular weight (MW) of pectin is a critical structural parameter governing yogurt texture through the precise modulation of casein-whey protein interactions. By employing ethanol fractionation to obtain pectin fractions with distinct MW values, we identified a non-linear, U-shaped textural evolution within the yogurt matrix. Specifically, the system transitions from firm gelation (Phase II, LP40) to flowable sol formation (Phase III, LP60), before returning to solid-like re-gelation (Phase IV, LP80). This U-shaped behavior is mechanistically driven by a strategic rebalancing of molecular forces: while the firm gels at the MW extremes (LP40 and LP80) are stabilized by enhanced disulfide bonding, the intermediate LP60 maintains its smooth, flowable consistency through dominant electrostatic repulsion. These findings demonstrate that ethanol fractionation provides a precise 'textural tailoring' toolkit. By strategically selecting the optimal pectin MW, it is possible to develop personalized dairy products, such as smooth-style yogurts for populations with dysphagia, with precisely tuned rheological properties. Ultimately, this work bridges the gap between polysaccharide molecular architecture and macroscopic food performance, advancing the integration of food science with human wellness.

Conflicts of interest

The authors declare no competing financial interest.

Acknowledgment

This research was supported by National Natural Science Foundation of China (U24A20466) and National Key R&D Program of China (2023YFD2100302).

Appendix A. Supplementary data

Supplementary material related to this article can be found in the online version, at https://doi.org/10.xxxx

References

[1] I. Ahmad, M. Hao, Y. Li, J. Zhang, Y. Ding, F. Lyu, Fortification of yogurt with bioactive functional foods and ingredients and associated challenges - A review, Trends Food Sci. Technol. 129 (2022) 558–580. https://doi.org/10.1016/j.tifs.2022.11.003.

[2] H. Du, X. Wang, H. Yang, F. Zhu, J. Cheng, X. Peng, Y. Lin, X. Liu, Effects of mulberry pomace polysaccharide addition before fermentation on quality characteristics of yogurt, Food Control 153 (2023) 109900. https://doi.org/10.1016/j.foodcont.2023.109900.

[3] H. Zhang, H.D. Goff, C. Liu, S. Luo, X. Hu, Blending pectin and κ-carrageenan converted the liquid yogurt induced by pectin into the solid yogurt, Carbohydr. Polym. 348 (2025) 122869. https://doi.org/10.1016/j.carbpol.2024.122869.

[4] H. Zhang, H.D. Goff, C. Liu, S. Luo, X. Hu, Preparation of liquid yogurt in the presence of pectin and its formation mechanism, Food Chem. 452 (2024) 139473. https://doi.org/10.1016/j.foodchem.2024.139473.

[5] X. Wang, E. Kristo, G. LaPointe, Adding apple pomace as a functional ingredient in stirred-type yogurt and yogurt drinks, Food Hydrocoll. 100 (2020) 105453. https://doi.org/10.1016/j.foodhyd.2019.105453.

[6] P.Y. Tan, T.B. Tan, H.W. Chang, B.T. Tey, E.S. Chan, O.M. Lai, B.S. Baharin, I.A. Nehdi, C.P. Tan, Effects of storage and yogurt matrix on the stability of tocotrienols encapsulated in chitosan-alginate microcapsules, Food Chem. 241 (2018) 79–85. https://doi.org/10.1016/j.foodchem.2017.08.075.

[7] J.A. Lucey, D.J. Wilbanks, D.S. Horne, Impact of heat treatment of milk on acid gelation, Int. Dairy J. 125 (2022) 105222. https://doi.org/10.1016/j.idairyj.2021.105222.

[8] J. Schulte, M. Stöckermann, R. Gebhardt, Influence of pH on the stability and structure of single casein microparticles, Food Hydrocoll. 105 (2020) 105741. https://doi.org/10.1016/j.foodhyd.2020.105741.

[9] K. Liu, Q.-M. Li, X.-Q. Zha, L.-H. Pan, L.-J. Bao, H.-L. Zhang, J.-P. Luo, Effects of calcium or sodium ions on the properties of whey protein isolate-lotus root amylopectin composite gel, Food Hydrocoll. 87 (2019) 629–636. https://doi.org/10.1016/j.foodhyd.2018.08.050.

[10] Y. Xiao, S. Kang, Y. Liu, X. Guo, M. Li, H. Xu, Effect and mechanism of calcium ions on the gelation properties of cellulose nanocrystals-whey protein isolate composite gels, Food Hydrocoll. 111 (2021) 106401. https://doi.org/10.1016/j.foodhyd.2020.106401.

[11] C.I. Vénica, I.V. Wolf, M.J. Spotti, M.L. Capra, D.J. Mercanti, M.C. Perotti, Impact of protein-providing milk ingredients on volatile compounds, microstructure, microbiology and physicochemical characteristics of yogurts, Food Biosci. 53 (2023) 102588. https://doi.org/10.1016/j.fbio.2023.102588.

[12] M. Yin, D. Yang, S. Lai, H. Yang, Rheological properties of xanthan-modified fish gelatin and its potential to replace mammalian gelatin in low-fat stirred yogurt, LWT - Food Sci. Technol. 147 (2021) 111643. https://doi.org/10.1016/j.lwt.2021.111643.

[13] Development and mechanical properties of soy protein fibrils-chitin nanowhiskers complex gel, Food Hydrocoll. 139 (2023) 108513. https://doi.org/10.1016/j.foodhyd.2023.108513.

[14] A.K. Rashwan, A.I. Osman, W. Chen, Natural nutraceuticals for enhancing yogurt properties: a review, Environ. Chem. Lett. 21 (2023) 1907–1931. https://doi.org/10.1007/s10311-023-01588-0.

[15]Z. Wan, S. Khubber, M. Dwivedi, N. Misra, Strategies for lowering the added sugar in yogurts, Food Chem. 344 (2021) 128573. https://doi.org/10.1016/j.foodchem.2020.128573.

[16] H. Gao, L. Ma, W. Sun, D.J. McClements, C. Cheng, H. Zeng, L. Zou, W. Liu, Impact of encapsulation of probiotics in oil-in-water high internal phase emulsions on their thermostability and gastrointestinal survival, Food Hydrocoll. 126 (2022) 107478. https://doi.org/10.1016/j.foodhyd.2021.107478.

[17] W. Song, Y. Wang, G. Li, S. Xue, G. Zhang, Y. Dang, H. Wang, Modulating the gut microbiota is involved in the effect of low-molecular-weight Glycyrrhiza polysaccharide on immune function, Gut Microbes 15 (2023) 2276814. https://doi.org/10.1080/19490976.2023.2276814.

[18] P. Ishwarya S., S. R., P. Nisha, Advances and prospects in the food applications of pectin hydrogels, Crit. Rev. Food Sci. Nutr. 62 (2022) 4393–4417. https://doi.org/10.1080/10408398.2021.1875394.

[19] S. Rawat, T. Pavithra, C.K. Sunil, Citrus byproduct valorization: pectin extraction, characterization, and research advances in biomaterial derivation for applications in active film packaging, Discov. Food 4 (2024) 149. https://doi.org/10.1007/s44187-024-00238-w.

[20] F. Gao, X. Mao, P. Wang, R. Wang, H. Li, H. Ma, C. Chen, S. Song, D. Li, The effect of degree of esterification of pectin on the grainy properties of post-heated fermented milk, Food Hydrocoll. 168 (2025) 111484. https://doi.org/10.1016/j.foodhyd.2025.111484.

[21] I.E. Benmebarek, D.J. González-Serrano, J.D. Bechtner, J.M. Galindo, M.M. Martínez, M.P. Sánchez-Verdú, W. Khalid, A. Moreno, Microwave-assisted subcritical water extraction of low methoxyl pectin from pistachio industry waste: Optimization, characterization, emulsification, and gelation mechanism, Carbohydr. Polym. 368 (2025) 124107. https://doi.org/10.1016/j.carbpol.2025.124107.

[22] A. Kaczmarska, P.M. Pieczywek, J. Cybulska, J. Cieśla, A. Zdunek, Structural and rheological properties of diluted alkali soluble pectin from apple and carrot, Food Chem. 446 (2024) 138869. https://doi.org/10.1016/j.foodchem.2024.138869.

[23] J. Liu, Z. Zhang, Y. Deng, G. Chen, Effect of extraction method on the structure and bioactivity of polysaccharides from activated sludge, Water Res. 253 (2024) 121196. https://doi.org/10.1016/j.watres.2024.121196.

[24] L. Hu, F. Ding, W. Liu, Y. Cheng, J. Zhu, L. Ma, Y. Zhang, H. Wang, Effect of enzymatic-ultrasonic hydrolyzed chitooligosaccharide on rheology of gelatin incorporated yogurt and 3D printing, Food Hydrocoll. 132 (2022) 107851. https://doi.org/10.1016/j.foodhyd.2022.107851.

[25] Y.-X. Chen, X.-Y. Liu, Z. Xiao, Y.-F. Huang, B. Liu, Antioxidant activities of polysaccharides obtained from Chlorella pyrenoidosa via different ethanol concentrations, Int. J. Biol. Macromol. 91 (2016) 505–509. https://doi.org/10.1016/j.ijbiomac.2016.05.086.

[26] K.P.B. Costa, L.H. Reichembach, C.L. De Oliveira Petkowicz, Pectins with commercial features and gelling ability from peels of Hylocereus spp, Food Hydrocoll. 128 (2022) 107583. https://doi.org/10.1016/j.foodhyd.2022.107583.

[27] Y. Zhu, H. Wang, T. Zhang, X. Zhang, C. Zhu, Characterization, antioxidant activity and *in vitro* digestion of hawthorn pectin prepared by gradient ethanol precipitation, Int. J. Biol. Macromol. 267 (2024) 131278. https://doi.org/10.1016/j.ijbiomac.2024.131278.

[28] F. Mariotti, D. Tomé, P.P. Mirand, Converting Nitrogen into Protein—Beyond 6.25 and Jones' Factors, Crit. Rev. Food Sci. Nutr. 48 (2008) 177–184. https://doi.org/10.1080/10408390701279749.

[29] T. Bitter, H.M. Muir, A modified uronic acid carbazole reaction, Anal. Biochem. 4 (1962) 330–334. https://doi.org/10.1016/0003-2697(62)90095-7.

[30] Michel. DuBois, K.A. Gilles, J.K. Hamilton, P.A. Rebers, Fred. Smith, Colorimetric Method for Determination of Sugars and Related Substances, Anal. Chem. 28 (1956) 350–356. https://doi.org/10.1021/ac60111a017.

[31] M. Pérez, I. Dominguez-López, R.M. Lamuela-Raventós, The Chemistry Behind the Folin–Ciocalteu Method for the Estimation of (Poly)phenol Content in Food: Total Phenolic Intake in a Mediterranean Dietary Pattern, J. Agric. Food Chem. 71 (2023) 17543–17553. https://doi.org/10.1021/acs.jafc.3c04022.

[32] X. Chen, H. Zhang, W. Du, L. Qian, Y. Xu, Y. Huang, Q. Xiong, H. Li, J. Yuan, Comparison of different extraction methods for polysaccharides from *Crataegus pinnatifida* Bunge, Int. J. Biol. Macromol. 150 (2020) 1011–1019. https://doi.org/10.1016/j.ijbiomac.2019.11.056.

[33] X. Hu, H.D. Goff, Fractionation of polysaccharides by gradient non-solvent precipitation: A review, Trends Food Sci. Technol. 81 (2018) 108–115. https://doi.org/10.1016/j.tifs.2018.09.011.

[34] L.C. Vriesmann, C.L. De Oliveira Petkowicz, Polysaccharides from the pulp of cupuassu (Theobroma grandiflorum): Structural characterization of a pectic fraction, Carbohydr. Polym. 77 (2009) 72–79. https://doi.org/10.1016/j.carbpol.2008.12.007.

[35] J. Chen, H. Cheng, Z. Zhi, H. Zhang, R.J. Linhardt, F. Zhang, S. Chen, X. Ye, Extraction temperature is a decisive factor for the properties of pectin, Food Hydrocoll. 112 (2021) 106160. https://doi.org/10.1016/j.foodhyd.2020.106160.

[36] L. Yin, W. Duan, Y. Chen, D. Chen, Y. Wang, S. Guo, J. Qin, Biodegradable hydrogel from pectin and carboxymethyl cellulose with Silibinin loading for lung tumor therapy, Int. J. Biol. Macromol. 243 (2023) 125128. https://doi.org/10.1016/j.ijbiomac.2023.125128.

[37] D. Sun, X. Chen, C. Zhu, Physicochemical properties and antioxidant activity of pectin from hawthorn wine pomace: A comparison of different extraction methods, Int. J. Biol. Macromol. 158 (2020) 1239–1247. https://doi.org/10.1016/j.ijbiomac.2020.05.052.

[38] Y. Dai, L. Wang, X. Chen, A. Song, L. He, L. Wang, D. Huang, Lentinula edodes Sing Polysaccharide: Extraction, Characterization, Bioactivities, and Emulsifying Applications, Foods 12 (2023) 3289. https://doi.org/10.3390/foods12173289.

[39] C. Chen, P. Wang, N. Zhang, W. Zhang, F. Ren, Improving the textural properties of camel milk acid gel by treatment with trisodium citrate and transglutaminase, LWT 103 (2019) 53–59. https://doi.org/10.1016/j.lwt.2018.12.063.

[40] L. Ji, Y. Xue, T. Zhang, Z. Li, C. Xue, The effects of microwave processing on the structure and various quality parameters of Alaska pollock surimi protein-polysaccharide gels, Food Hydrocoll. 63 (2017) 77–84. https://doi.org/10.1016/j.foodhyd.2016.08.011.

[41] Y. Li, M. Cai, S. Ma, H. Lu, X. Liu, Heat-induced gel formation by whey protein isolate-deacetylated konjac glucomannan at varying pH conditions, Food Hydrocoll. 145 (2023) 109076. https://doi.org/10.1016/j.foodhyd.2023.109076.

[42] X. Chen, Y. Qi, C. Zhu, Q. Wang, Effect of ultrasound on the properties and antioxidant activity of hawthorn pectin, Int. J. Biol. Macromol. 131 (2019) 273–281. https://doi.org/10.1016/j.ijbiomac.2019.03.077.

[43] H. Han, Y. Luo, J. Bai, Z. Tao, S. Wang, X. Lei, Y. Feng, Y. Ren, Electron beam irradiation pretreatment for efficient extraction of pectin from spaghetti squash peel: Structural, functional, and biological properties, Food Hydrocoll. 148 (2024) 109451. https://doi.org/10.1016/j.foodhyd.2023.109451.

[44] Z. Yang, Y. Hu, P. Yue, H. Luo, Q. Li, H. Li, Z. Zhang, F. Peng, Physicochemical Properties and Skin Protection Activities of Polysaccharides from Usnea longissima by Graded Ethanol Precipitation, ACS Omega 6 (2021) 25010–25018. https://doi.org/10.1021/acsomega.1c04163.

[45] Z. Košťálová, Z. Hromádková, Structural characterisation of polysaccharides from roasted hazelnut skins, Food Chem. 286 (2019) 179–184. https://doi.org/10.1016/j.foodchem.2019.01.203.

[46] X. Yang, S. Wei, X. Lu, X. Qiao, J. Simal-Gandara, E. Capanoglu, Ł. Woźniak, L. Zou, H. Cao, J. Xiao, X. Tang, N. Li, A neutral polysaccharide with a triple helix structure from ginger: Characterization and immunomodulatory activity, Food Chem. 350 (2021) 129261. https://doi.org/10.1016/j.foodchem.2021.129261.

[47] S.T. Minzanova, V.F. Mironov, A.B. Vyshtakalyuk, O.V. Tsepaeva, L.G. Mironova, A.Z. Mindubaev, I.R. Nizameev, K.V. Kholin, V.A. Milyukov, Complexation of pectin with macro- and microelements. Antianemic activity of Na, Fe and Na, Ca, Fe complexes, Carbohydr. Polym. 134 (2015) 524–533. https://doi.org/10.1016/j.carbpol.2015.07.034.

[48] X. Gao, J. Qi, C.-T. Ho, B. Li, J. Mu, Y. Zhang, H. Hu, W. Mo, Z. Chen, Y. Xie, Structural characterization and immunomodulatory activity of a water-soluble polysaccharide from *Ganoderma leucocontextum* fruiting bodies, Carbohydr. Polym. 249 (2020) 116874. https://doi.org/10.1016/j.carbpol.2020.116874.

[49] J. Zhang, Y. Li, W. Li, L. Zhou, Y. Lan, J. Guo, The synergistic trigger of the reductive dissolution of Schwertmannite-As(III) and the release of arsenic from citric acid and UV irradiation, Chem. Geol. 520 (2019) 11–20. https://doi.org/10.1016/j.chemgeo.2019.05.004.

[50] L.R. Adetunji, A. Adekunle, V. Orsat, V. Raghavan, Advances in the pectin production process using novel extraction techniques: A review, Food Hydrocoll. 62 (2017) 239–250. https://doi.org/10.1016/j.foodhyd.2016.08.015.

[51] A. Zdunek, P.M. Pieczywek, J. Cybulska, The primary, secondary, and structures of higher levels of pectin polysaccharides, Compr. Rev. Food Sci. Food Saf. 20 (2021) 1101–1117. https://doi.org/10.1111/1541-4337.12689.

[52] L. Yang, L.-M. Zhang, Chemical structural and chain conformational characterization of some bioactive polysaccharides isolated from natural sources, Carbohydr. Polym. 76 (2009) 349–361. https://doi.org/10.1016/j.carbpol.2008.12.015.

[53] X. Guo, J. Kang, Z. Xu, Q. Guo, L. Zhang, H. Ning, S.W. Cui, Triple-helix polysaccharides: Formation mechanisms and analytical methods, Carbohydr. Polym. 262 (2021) 117962. https://doi.org/10.1016/j.carbpol.2021.117962.

[54] Y. Wang, A. Zhang, W. Zhao, J. Liu, H. Yi, Effect of triple helix polysaccharides from foxtail millet bran on millet starch gel formation, Int. J. Biol. Macromol. 304 (2025) 140796. https://doi.org/10.1016/j.ijbiomac.2025.140796.

[55] Y. Xiao, S. Liu, M. Shen, L. Jiang, Y. Ren, Y. Luo, H. Wen, J. Xie, Physicochemical, rheological and thermal properties of *Mesona chinensis* polysaccharides obtained by sodium carbonate assisted and cellulase assisted extraction, Int. J. Biol. Macromol. 126 (2019) 30–36. https://doi.org/10.1016/j.ijbiomac.2018.12.211.

[56] H. Li, Z. Li, P. Wang, Z. Liu, L. An, X. Zhang, Z. Xie, Y. Wang, X. Li, W. Gao, Evaluation of citrus pectin extraction methods: Synergistic enhancement of pectin's antioxidant capacity and gel properties through combined use of organic acids, ultrasonication, and microwaves, Int. J. Biol. Macromol. 266 (2024) 131164. https://doi.org/10.1016/j.ijbiomac.2024.131164.

[57] W. Yao, M. Liu, X. Chen, L. You, Y. Ma, K. Hileuskaya, Effects of UV/H2O2 degradation and step gradient ethanol precipitation on *Sargassum fusiforme* polysaccharides: Physicochemical characterization and protective effects against intestinal epithelial injury, Food Res. Int. 155 (2022) 111093. https://doi.org/10.1016/j.foodres.2022.111093.

[58] S. Ma, S. Yu, X. Zheng, X. Wang, Q. Bao, X. Guo, Extraction, characterization and spontaneous emulsifying properties of pectin from sugar beet pulp, Carbohydr. Polym. 98 (2013) 750–753. https://doi.org/10.1016/j.carbpol.2013.06.042.

[59] K. Arab, B. Ghanbarzadeh, A. Ayaseh, K. Jahanbin, Extraction, purification, physicochemical properties and antioxidant activity of a new polysaccharide from *Ocimum album* L. seed, Int. J. Biol. Macromol. 180 (2021) 643–653. https://doi.org/10.1016/j.ijbiomac.2021.03.088.

[60] G. You, X.L. Liu, M.M. Zhao, Preparation and characterization of hsian-tsao gum and chitosan complex coacervates, Food Hydrocoll. 74 (2018) 255–266. https://doi.org/10.1016/j.foodhyd.2017.08.004.

[61] X. Kang, S. Jia, W. Gao, B. Wang, X. Zhang, Y. Tian, Q. Sun, M. Atef, B. Cui, A.M. Abd El-Aty, The formation of starch-lipid complexes by microwave heating, Food Chem. 382 (2022) 132319. https://doi.org/10.1016/j.foodchem.2022.132319.

[62] H. Sıçramaz, Synergistic effect of ultrasound and pectin addition on enhancing yogurt structure, LWT - Food Sci. Technol. 228 (2025) 118082. https://doi.org/10.1016/j.lwt.2025.118082.

[63] X. Qin, X. Wu, C. Yu, Y. Chai, X. Liu, X. Zhang, H. Cai, M. Lai, L. Qiu, Y. Hao, R. Wang, Y. Li, P. Wang, H. Li, X. Wang, Post-heat treatment and pectin addition affect protein digestion and absorption release kinetics in pigs through microstructural and rheological modifications, Food Chem. 492 (2025) 145502. https://doi.org/10.1016/j.foodchem.2025.145502.

[64] A. Syrbe, W.J. Bauer, H. Klostermeyer, Polymer Science Concepts in Dairy Systems—an Overview of Milk Protein and Food Hydrocolloid Interaction, Int. Dairy J. 8 (1998) 179–193. https://doi.org/10.1016/S0958-6946(98)00041-7.

[65] K. Watanabe, Y. Tajima, T. Shimura, H. Ishii, D. Nagao, Depletion-interaction-driven assembly of golf ball-like particles for development of colloidal macromolecules, J. Colloid Interface Sci. 534 (2019) 81–87. https://doi.org/10.1016/j.jcis.2018.08.117.

[66] P. Methacanon, C. Gamonpilas, A. Kongjaroen, C. Buathongjan, Food polysaccharides and roles of rheology and tribology in rational design of thickened liquids for oropharyngeal dysphagia: A review, Compr. Rev. Food Sci. Food Saf. 20 (2021) 4101–4119. https://doi.org/10.1111/1541-4337.12791.

[67] O. Jones, E.A. Decker, D.J. McClements, Thermal analysis of β-lactoglobulin complexes with pectins or carrageenan for production of stable biopolymer particles, Food Hydrocoll. 24 (2010) 239–248. https://doi.org/10.1016/j.foodhyd.2009.10.001.

[68] Y. Jia, J. Du, K. Li, C. Li, Emulsification mechanism of persimmon pectin with promising emulsification capability and stability, Food Hydrocoll. 131 (2022) 107727. https://doi.org/10.1016/j.foodhyd.2022.107727.

[69] E. Dickinson, Exploring the frontiers of colloidal behaviour where polymers and particles meet, Food Hydrocoll. 52 (2016) 497–509. https://doi.org/10.1016/j.foodhyd.2015.07.029.

[70] W. Liang, J. Liao, J.-R. Qi, W. Jiang, X. Yang, Physicochemical characteristics and functional properties of high methoxyl pectin with different degree of esterification, Food Chem. 375 (2022) 131806. https://doi.org/10.1016/j.foodchem.2021.131806.

[71] W. Tang, X. Lin, L. Ye, J. He, Z. Wang, J. Tang, J. Liu, P. Zhao, Effect of pectin with different esterification degree on the freeze-thaw stability of gluten protein: Structures, functional properties, and Cryoprotective mechanism, Food Chem. 465 (2025) 142040. https://doi.org/10.1016/j.foodchem.2024.142040.

[72] C.G. de Kruif, R. Tuinier, Polysaccharide protein interactions, Food Hydrocoll. 15 (2001) 555–563. https://doi.org/10.1016/S0268-005X(01)00076-5.

[73] G. Tabilo-Munizaga, G.V. Barbosa-Cánovas, Rheology for the food industry, J. Food Eng. 67 (2005) 147–156. https://doi.org/10.1016/j.jfoodeng.2004.05.062.

[74] A.N. Hassan, R. Ipsen, T. Janzen, K.B. Qvist, Microstructure and Rheology of Yogurt Made with Cultures Differing Only in Their Ability to Produce Exopolysaccharides, J. Dairy Sci. 86 (2003) 1632–1638. https://doi.org/10.3168/jds.S0022-0302(03)73748-5.

[75] A. Krzeminski, K. Großhable, J. Hinrichs, Structural properties of stirred yoghurt as influenced by whey proteins, LWT - Food Sci. Technol. 44 (2011) 2134–2140. https://doi.org/10.1016/j.lwt.2011.05.018.

[76] M.R.S. Leal, P.B.S. Albuquerque, N.E.R. Rodrigues, P.M. dos S. Silva, W.F. de Oliveira, M.T. dos S. Correia, J.F. Kennedy, L.C.B.B. Coelho, A review on the use of polysaccharides as thickeners in yogurts, Carbohydr. Polym. Technol. Appl. 8 (2024) 100547. https://doi.org/10.1016/j.carpta.2024.100547.